INDUSTRIAL SCREEN-PRINTED SOLAR CELLS WITH NOVEL ATMOSPHERIC PRESSURE DRY TEXTURING PROCESS

[1]Bishal Kafle, [1]Daniel Trogus, [2]Birte Dresler, [2]Daniel Köhler, [2]Gerrit Mäder, [3]Laurent Clochard, [3]Edward Duffy, [1]Marc Hofmann and [1]Jochen Rentsch
[1]Fraunhofer-Institute for Solar Energy Systems (ISE)
[2]Fraunhofer Institute for Material Beam Technology (IWS)
[3] Nines Photovoltaics
[1]Heidenhofstr. 2, 79110 Freiburg, Germany
[2]Winterbergstr.28, D-01277 Dresden, Germany
[3] IT Tallaght, Dublin 24, Ireland
Correspondence: bishal.kafle@ise.fraunhofer.de, +49 (0) 761 4588-9051

ABSTRACT:

Reduction of surface reflection remains a key area of investigation in order to improve the light confinement of solar cells. Our one step atmospheric pressure dry etching process uses F_2 gas to form nanotextures of different aspect ratios on c-Si surfaces. The developed process is expected to be economically competitive with wet-chemical texturing methods when scaled up for higher throughputs in an inline process. We have managed to reduce the weighted surface reflection dramatically up to 2% and this can potentially be lowered further.. We have optimized the surface texture that can be effectively passivated with ALD Al_2O_3 with reasonably low values of surface recombination velocities. First Al-BSF solar cells prepared on multicrystalline wafers using the non-optimized version of texture have reached a maximum conversion efficiency of 15.2% and primarily suffer with high recombination losses in the surface and emitter region. Our next generation solar cells with an optimized texture are expected to have significant improvement in the cell performance.

Keywords: Etching, Passivation, Texturisation

1 INTRODUCTION

Submicron texture with nanoscale dimension has a tremendous ability to surpass the light absorption limit of the standard wet-chemical texture in PV industry. Depending upon the feature size, the sub-micron texture can effectively reduce the surface reflection properties of crystalline Silicon (c-Si) by either acting as a graded density layer or by increasing the optical path length [1]. For multicrystalline silicon (mc-Si) solar cells, the industry standard still is the wet chemical so-called isotexture process that strongly lacks behind the alkaline texture process for monocrystalline wafers. Techniques that have been reported so far to produce nanoscale texture include dry texturing methods such as reactive ion etching [2, 3], femtosecond laser pulse texturing [4] as well as wet chemical methods such as metal nanoparticle assisted etching [5]. The dry processing methods however are supposed to have clear advantages over wet-chemical methods both economically and environmentally, especially for a large scale industrial manufacturing plant.

We have investigated a novel atmospheric pressure (AP) dry etching process that uses molecular fluorine (F_2) gas to texture c- Si surfaces for solar cell applications [6]. The texturing process does not need any plasma source or costly vacuum pumps. An atmospheric pressure process therefore provides a huge cost advantage compared to other existing alternatives. Large amount of F_2 gas used in other industries suggest that it can well be scaled up to be used in large scale PV manufacturing plants [7]. F_2 is a non-global warming potential (GWP) gas, thus fits perfectly with the long-time roadmap of a sustainable PV industry.

Thermally activated F_2 gas reacts with Si and can form nanoscale structures with different aspect ratios. If the dimensions of the nanotexture are comparable to the wavelength of incident light, the reflection from the Si surface is suppressed comprehensively. As the depth of the nanostructure increases, most of the incident light is absorbed in the Si surface and it ultimately looks black in colour, thus named as 'Black Silicon' (B-Si). Although B-Si utilizes a very high percentage of incident light for the photogeneration of charge carriers, it also suffers with an increased surface recombination due to a large total surface area. An increased surface area also leads to a higher number of dopants in the emitter region. The dimensions of the nanotexture might need some adjustment of the screen printing process, which still is the most common way of forming metal contacts in a solar cell. Therefore, it remains a challenge to fabricate nanotextured solar cells that follow the same process steps as the standard cells textured with wet chemistry.

In this paper, we present a novel atmospheric pressure dry texturing process based upon thermally activated F_2 gas. The mechanism of the dry etching process is discussed briefly and the detailed outline of the surface morphology is studied by the help of scanning electron beam microscopy (SEM) investigations. Optical performance of such a texture is presented and

measures to passivate very fine nanostructures are suggested as well. Al-BSF solar cells are fabricated for the first time with the dry textured wafers by keeping most of the other standard cell process steps intact. The cell results are analysed and guidelines for the improvement of the cell performance are also suggested.

2 ATMOSPHERIC PRESSURE DRY ETCHING

The etching is performed in an atmospheric pressure etching tool that uses F_2 as the etching gas. For this study, the tool was set up to work with the maximum of 20 % of F_2 diluted in 80% of N_2. The diluted F_2 is heated at a gas diffusion plate (GDP) for thermal dissociation into F atoms. The Si wafer is fixed in the wafer holder and is also heated up to certain temperatures that are supposed to increase the reaction rate. The etching reaction occurs in the reaction zone at nearly atmospheric pressure conditions. No gaseous exchange between inside and outside of the reaction zone is allowed due to the slight difference of the pressure between the zones and gas curtains. During the etching process, the wafer moves with a certain speed through the etching zone. The etching of Si is therefore a dynamic process.

2.1 Mechanism of etching

F atoms are weakly bonded in a non-polar covalent bond with a bond length of 1.42 A° to form a F_2 molecule [8]. A very high electronegativity of F atom suggests that that surpassing a low bonding energy of F_2 is relatively easy and results in an exothermic reaction. Though the dissociation of F_2 into F atoms is thermodynamically favourable even with low energies, a relatively low temperature of 300°C used in our tool settings might be able only to partially dissociate F_2 gas while it is heated in the gas diffusion plate before reaching the Si substrate. The main etching reaction occurs at the Si surface and F_2/F reacts spontaneously with the Si surface. A simple reaction mechanism as suggested by previous studies follows three main steps – the first mechanism being chemisorption of the F_2/F at Si surface dangling bonds, second being formation of a Fluorosilyl layer in the first 10-30 Å of Si surface and third being the desorption of SiF_x species from the Si surface [9, 10]. Since the spontaneous reaction systems are limited due to the surface reaction kinetics, substrate temperature plays a big role in etching process [11]. A higher substrate temperature possibly enhances the chemisorption of F/F_2 onto the Si and/or increases the rate of formation and desorption of SiF_x species. Based upon the substrate temperature, any of the first and third steps could be the rate limiting step. The reaction products are SiF_x species, most possibly

with a higher mix of SiF_4 in the range of substrate temperatures used in these studies [12].

2.2 Morphology and optical properties of the nanotexture

The main process parameters of the dry etching tool used in this study are input gas flux (F_2 + N_2), F_2 concentration delivered in the etching zone, speed with which the wafer travels through etching zone, temperature of the GDP and substrate temperature. Different combinations of process parameters end up with different etch rates and texture morphologies. We have achieved highly controlled anisotropic etching of Si by thermally activated F_2. The anisotropy is the result of a self-masking effect in F_2-Si reaction mechanism that has been exploited to create anisotropic structures with different aspect ratios. This self-masking effect possibly is the result of initial localized reaction of F_2 with Si at certain locations and forming microscopic areas with local higher temperature and an increased roughness, thus enhancing more etching at these locations. The exact mechanism of self-masking is however still not clear and is a topic of investigation.

Figure 1 shows nanostructures of different aspect ratios. Based upon amount of Si removed during the texturing step, they are classified as very shallow, shallow, intermediate and deep nanostructures.
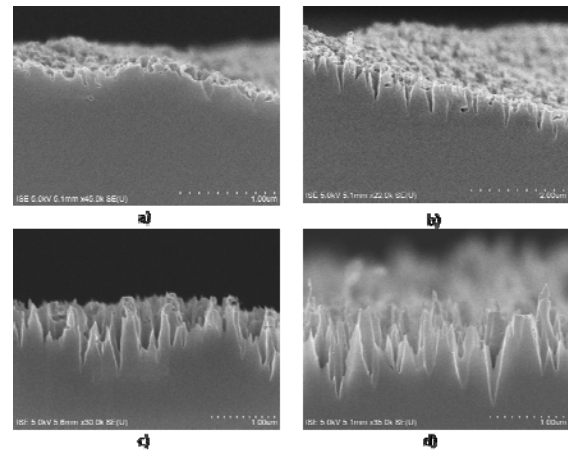

Figure 1: SEM cross-sectional overview of the nanotexture formed in c-Si with a crystal orientation of (100): – a) very shallow nanotexture, b) shallow B-Si, c) intermediate B-Si and d) deep B-Si. The different surface roughnesses lead to the formation of light trapping structures with different surface reflections.

Image a) shows the surface texture created by removing only 0.35 µm on average of Si resulting in very shallow nanostructures with occasional deeper valleys in the silicon. Image b) shows the shallow texture created by removing ~0.8 µm on average of Si to form inverted valley-like structures. Images c) and d) are the surface textures

formed by removing ~1.2 µm and ~2.9 µm of Si with randomly sized needle like structures or so called B-Si. These B-Si structures consist of spikes of varying height principally in <100> direction with very sharp edges and occasional tunnelling into <010> and <001>. The structures typically size from 500 – 1000 nm in depth and 200 – 500 nm in width depending on the applied etching conditions.

Spectral reflection of the different nanotextures in the spectral range of 250-1200 nm is measured by spectrophotometer considering the incident light normal to the textured surface. Figure 2 summarizes the reflection plots of B-Si structures and compares them to the reference pyramid texture. Averaged weighted reflection values R_w are also calculated for the same spectral range [13]. As observed previously in other studies [14], the depth of the nanostructures is found to have an inverse correlation to the surface reflection. The very shallow and shallow nanostructures suffer from relatively high surface reflection of ~14% and ~ 10% respectively. Because of having deep nanostructures featuring an increase in graded index of refraction from air to Si, the intermediate and deep B-Si structures can reach a much lower weighted surface reflection of ~5% and ~2% respectively. For reference, the alkaline texture has an average weighted surface reflection of ~11%. The nanotexturing also provides a possibility of reaching very low surface reflection values very small amounts of Si being removed from the substrate. For comparison, 0.7 – 0.8 µm removal of Si provides similar weighted reflection as a wet chemical alkaline texture that removes ~7 µm of Si. A removal of very small amount of Si during texturing process is of high importance for advanced cell concepts that uses thinner wafers and also for the economical cell concepts that make use of thin epitaxial Si layers grown on top of low-cost substrates.
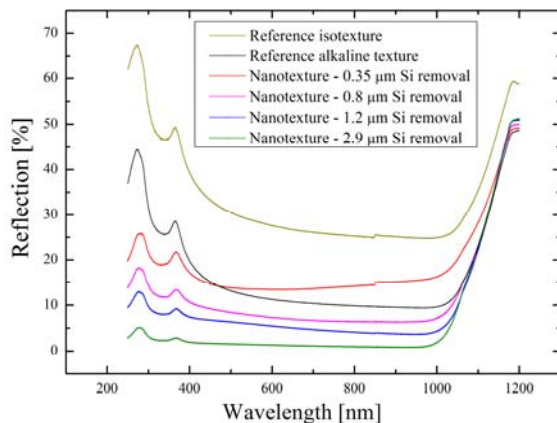

Figure 2: Comparison of the surface reflection spectra for the nanostructures formed with different surface morphology. In comparison, reflection from the alkaline wet chemical texture and acidic isotexture has also been plotted.

2.3 Surface passivation of the nanotexture

By virtue of having a larger surface area and therefore higher surface defect states, nanotexture suffers from higher recombination of minority charge carriers compared to non-textured surfaces. An increasing graded index depth further complicates the issue of surface passivation due to the inability of the most common deposition techniques such as chemical vapour deposition (CVD), plasma enhanced chemical vapour deposition (PECVD) and sputtering to form conformal dielectric layers that are typically used for antireflective and passivation purposes. Typical front side dielectric layers used in standard industrial cell processes are therefore incompatible with the nanotexture. However, since the nanotextured surface with very low surface reflection does not need any antireflection layer, this provides more freedom with the selection of dielectric layers for passivation.

Atomic layer deposition (ALD) is widely reported as a deposition technique that provides an advantage of growing extremely conformal thin layers of well-defined thickness [15]. Thin ALD Al_2O_3 layers form excellent chemical interface with Si minimizing the interface defect density (D_{it}). Inherent negative charge present in the Al_2O_3 layers also provides an excellent field effect passivation. Due to its conformity and excellent passivation properties, they are well suited for the structures having nanoscale dimensions.

We have deposited stacks of plasma assisted ALD Al_2O_3 and PECVD SiN_x in the nanostructures formed by our etching mechanism. P-type float zone (FZ) wafers with base resistivity of 1 Ω cm were first treated to remove the saw damages on the surface of the wafer and then textured on both sides with thermally activated F_2 at the substrate temperature of 200°C with the wafer moving with different velocity through the reaction zone to form nanostructures of different dimensions. After the texturing process, the wafers were cleaned using standard RCA cleaning [16]. After the cleaning, a group of wafer was additionally pre-conditioned in hot HNO_3 bath for 10 minutes to form a wet-chemical oxide layer. Symmetrical lifetime samples were prepared by depositing stacks of ALD Al_2O_3 and PECVD SiN_x on both sides of the wafer. The samples were subsequently subjected to a firing process at a peak temperature of 880°C for ~3 seconds in an industrially applicable fast firing oven. Effective lifetimes of the minority charge carriers (τ_{eff}) were measured for the samples using quasi steady state photo-conductance decay (QSSPC) method in generalized mode of measurement.

The first lifetime experiment was done prior to any optimization of the etching process. After optimization of the process parameters, the lifetime

experiments were performed again. Though possessing very good reflection properties, the nanostructures created by the non-optimized process had a high level of inherent porosity with apparently no well-defined structures, with nanoscale roughness also visible that gives it a 'spongy' appearance in SEM. Figure 3 compares the surface morphology of the nanostructures formed as a result of previous non-optimized process to those created with an optimized process.
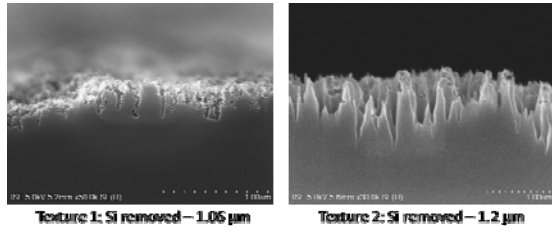

Figure 3: Comparison of the texture 1 formed by applying a non-optimized process with the texture 2 formed using an optimized texture process to form B-Si like nanostructures. The weighted reflection for texture 1 and texture 2 are 5.9 % and 5.5 % respectively.

The inherent porosity of texture 1 resulted in a higher number of surface defect states. Additionally the surface roughness with dimensions in tens of nanometres made it an extremely difficult surface for passivation. Therefore texture 1exhibits very high surface recombination velocity as compared to texture 2. Figure 4 compares the surface recombination velocity of the non-optimized texture 1 to the texture 2 formed using optimized process parameters. Assuming an infinite bulk lifetime of FZ wafers used for the experiments, the maximum value of surface recombination velocity ($S_{eff,max}$) was calculated for the symmetrical samples by using the equation [17].

$$S_{eff,max} = \frac{W}{2 \times \tau_{eff}},$$

where, W is the wafer thickness and τ_{eff} is the effective lifetime obtained from quasi-steady state photo-conductance decay (QSSPC) method. Additionally, while deriving $S_{eff,max}$ for the single sided textured samples, it has been assumed that the non-textured side of the wafer is perfectly passivated with no surface recombination.

Figure 5 plots the surface recombination velocities that are calculated on the symmetrically textured wafers with different amount of Si removed during the texturing process. This implies that a stack layer of ALD Al_2O_3 and PECVD SiN_x on preconditioned Si surface provides a very good passivation, even for intermediate and deep nanostructures.
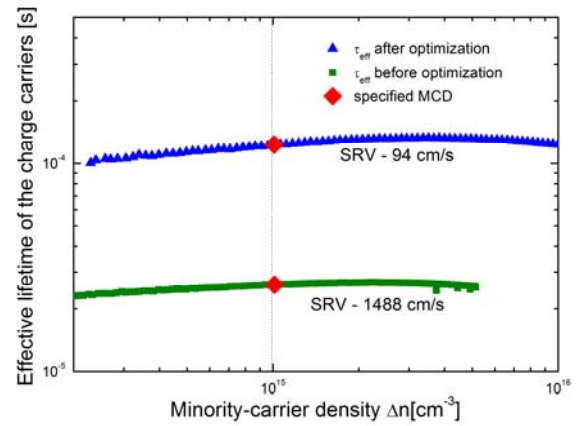

Figure 4: Comparison of the passivation between texture 1 and texture 2 based effective carrier lifetime measurement data plotted at different carrier injection levels. The textured surfaces of both samples were then passivated with a stack of 10 nm ALD Al_2O_3 and 70 nm PECVD SiN_x. The wafers with texture 1 and texture 2 were textured on one side and both sides of the wafer respectively.
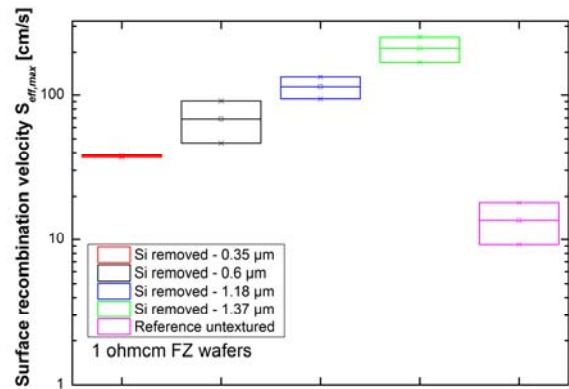

Figure 5: $S_{eff,max}$ calculated for dry texture with various amounts of Si removed are plotted alongside that for the plain reference sample.

Figure 6 shows the SEM cross-section of intermediate B-Si–like texture coated with the Al_2O_3/SiN_x stack of passivation layers as stated before. From SEM overview, it is obvious that ALD Al_2O_3 layers reach out even in very deep valleys and form a very conformal passivation layer covering every surface of the nanostructures. PECVD SiN_x layers however stay on top of the nanostructure but are not able to form a conformal passivation layer.
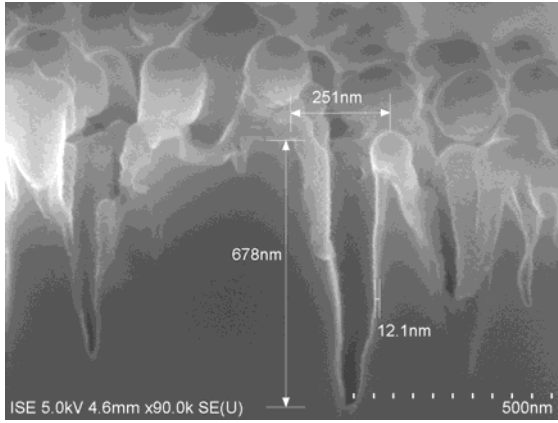
Figure 6: SEM cross-section showing intermediate nanostructures passivated with 10 nm of p-ALD Al_2O_3 and 70 nm of PECVD SiN_x. The ALD deposition forms a conformal layer covering most of the surface of the nanostructure while the stacked PECVD SiN_x layer cannot reach the deep valleys.

3 FIRST DRY TEXTURED SCREEN PRINTED SOLAR CELLS

While still optimizing the surface morphology of the dry texture, we made the first Al-BSF solar cells of multicrystalline (mc) wafers using the non-optimized texture that was compared with an optimized texture in Figure 3. Figure 6 provides a brief overview of the cell process steps.

Figure 7: Process plan followed for Al-BSF solar cells textured by atmospheric pressure dry etching process.

Dry texture was applied both on saw damage etched surfaces and on isotextured surfaces. Isotextured wafers were used as the references for the comparison of the performance of the dry textured cells to the industrially manufactured mc solar cells. As shown in Figure 8, the dry textured multicrystalline wafers possess very good optical properties as compared to the wet-chemically isotextured wafers. Hence, the dry textured structures with 200-600 nm depth and 50-100 nm width are found to be extremely well suited for the light confinement in case of multicrystalline wafers.

The wafers were cleaned before the tube diffusion process and then were diffused with 70 $\Omega/\square$ n-type emitter. After etching of PSG layer, the front side of the wafers were passivated with a stack of 10 nm ALD Al_2O_3 and 70 nm PECVD SiN_x. Metallization was done by screen printing of front and rear surfaces followed by the co-firing step to form metal-Si contacts.
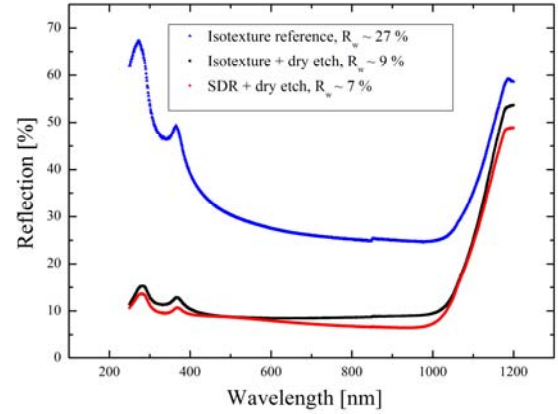

Figure 8: Comparison of surface reflection of multicrytalline wafers showing dry textured surface and reference isotexture surface.

Table 1 summarizes the IV characteristics of the Al-BSF cells.

	V_{oc} (mV)	J_{sc} (mAcm^{-2})	FF (%)	η (%)
Gr. 1	602	32.2	77.6	15.2
Gr. 2	603	31.3	75.3	14.2
Reference	615	34.1	78.8	16.4

Table 1: IV characteristics of Al-BSF cells applying short isotexture process + dry etching (Gr.1), saw damage etching + dry etching (Gr. 2) and isotexture reference process.

The results from the first batch of solar cells suggest that the electrical behaviour of the AP dry textured cell is significantly hampered due to a high surface and Auger recombination in the emitter region of the cell. A lowered V_{oc} is mainly attributed to a high saturation current density (j_0) of dry textured cells primarily due to heavy charge carrier recombination in the emitter region. Sheet resistance mapping on the full wafer area also revealed an inhomogeneous distribution with an overall doping higher than in reference acidic textured cells. An increment in the surface area facilitated easier diffusion of the dopant atoms into the Si bulk and resulted in heavier doping of the Si substrate. Highly doped emitter could also feature surface regions with very high concentration of electrically inactive phosphorous atoms, therefore making Shockley-Read-Hall recombination a

dominant recombination mechanism acting in parallel to the surface recombination mechanism. This has resulted in the poor blue response as shown in Figure 9. This has also lead to a loss of J_{sc} despite possessing excellent optical properties.
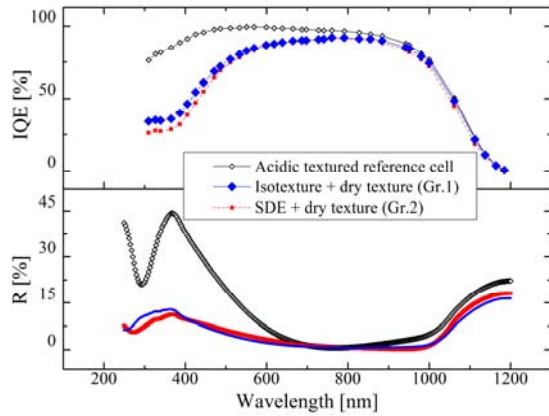

Figure 9: Internal quantum efficiency (IQE) and surface reflection (R) plotted for the wavelength spectrum of 250 nm – 1200 nm.

The dry textured cells also showed lower *FF* values as compared to the reference cells. The effect was much pronounced in the case of wafers that were saw damage etched before applying dry texturing. Series resistance (R_s) mapping of such a cell using the coupled determination of the dark saturation current and series resistance (C-DCR) method showed high R_s in a large section of the cell [18]. This could be partly attributed to the inhomogeneous diffusion of the dopants in the wafer area, partly to an inadequate formation of front contacts. Transmission line measurements (TLM) at different sections of the wafer confirmed very high contact resistances (R_c) in the middle large section of the solar cell.
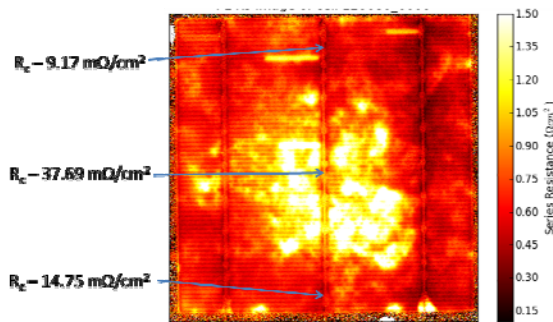

Figure 10: High contact resistance observed in the large section of wafer analysed by C-DCR method.

The distribution of the ohmic power loss of the cell is another way to verify the major problems. Application of the one dimensional simulation approach to obtain power loss distribution, as described by Jäger et al. [19] suggests that the power loss in the semiconductor-metal interface

represents a significant proportion of the total power loss, thus effectively lowering the overall *FF* of the cell.
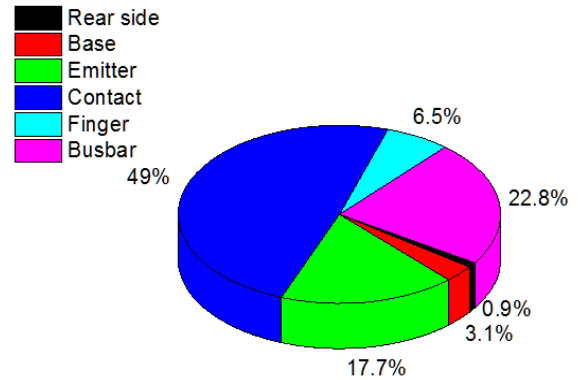

Figure 11: Ohmic power loss distribution of the dry textured solar cell (Gr. 2). Approximation for the value of recombination current in metal-Si contact was made in order to have convergence of the one dimensional simulation approach, resulting in the similar values of output parameters (V_{oc}, J_{sc}, *FF*, η) that were experimentally obtained by current-voltage (I-V) measurements. The lumped series resistance is calculated in order to obtain total power loss, and two-diode model is used to extract the *FF* of the cell.

4   SUMMARY

In summary, we presented a novel dry etching technology that works with thermally excited F_2 gas to form density graded nanostructures in a one step process. We showed that nanostructures of different surface morphology and aspect ratios can be formed by changing the etching conditions. The nanostructures formed are capable of very good optical confinement and were able to reach a very low weighted surface reflection value of 2%. The surface reflection can be further lowered using higher concentration of F_2 gas. We showed that despite having very large surface area of the dry textured structures, they can be effectively passivated by applying thin layers of ALD Al_2O_3. Finally, we demonstrated the results of our first Al-BSF solar cells made on multicrystalline wafers applying the dry atmospheric pressure texturisation process. The dry textured cells showed significant losses in the electrical behaviour in comparison to the reference isotextured cell. Application of a non-optimized dry texture process is supposed to have increased the surface area tremendously leading to higher doping and therefore more Auger and Shockley-Read-Hall recombination. In addition, a very rough surface also affected the conformability of the surface passivation layer and therefore suffers from surface recombination of the charge carriers. A lowered FF is supposedly because of the inhomogeneous distribution of the dopants and the result of non-optimized contact formation conditions. Although having lower performance than the isotextured reference cells, an efficiency of

15.2% on our first generation non-optimized dry textured cell is promising.

In our recent results, we have optimized the etching conditions and surface passivation, which has lowered the surface recombination velocity of the resulting texture by more than one magnitude. Using the optimized texture, we are expecting to have significant improvement in the electrical performance of the next generation dry textured cells.

5 ACKNOWLEDGEMENTS

6 REFERENCES

1. Stephens, R.B. and G.D. Cody, *OPTICAL REFLECTANCE AND TRANSMISSION OF A TEXTURED SURFACE.* Thin Solid Films, 1977. **45**: p. 19-29.
2. Garnett, E. and P. Yang, *Light Trapping in Silicon Nanowire Solar Cells.* Nano Lett., 2010. **10**(3): p. 1082 - 1087.
3. Lüdemann, R., et al. *Silicon solar cells with black silicon texturization.* in *Proceedings of the 17th European Photovoltaic Solar Energy Conference.* 2001. Munich, Germany: WIP-Munich and ETA-Florence.
4. Kontermann, S., et al. *Laser Processed Black Silicon for Photovoltaic Applications.* in *SiliconPV.* 2012. Leuven, Belgium.
5. Branz, H.M., et al., *Nanostructured black silicon and the optical reflectance of graded-density surfaces.* Appl. Phys. Lett., 2009. **94**(231121).
6. Dresler, B., et al. *Novel Industrial Single Sided Dry Etching and Texturing Process for Silicon Solar Cell Improvement.* in *27th EUPVSEC.* 2012. Frankfurt.
7. Groult, H., et al., *Role of elemental fluorine in nuclear field.* Journal of Fluorine Chemistry, 2007. **128**(4): p. 285 - 295.
8. Gray, H.B., *Chemical bonds: an introduction to atomic and molecular structure* 1994, CA: Universtiy Science Books.
9. Winters, H.F. and D. Haarer, *Influence of doping on the etching of Si (111).* PHYSICAL REVIEW B, 1987. **36**(12).
10. Garrison, B.J. and W.A.G. III, *Reaction mechanism for fluorine etching of silicon.* PHYSICAL REVIEW B, 1987. **36**(18).
11. Chen, F.F. and J.P. Chang, *LECTURE NOTES ON PRINCIPLES OF PLASMA PROCESSING.* 2003, New York: Plenum Publishers.
12. Bäuerle, D., *Laser Processing and Chemistry.* 2011, Springer-Verlag: Berlin Heidelberg. p. 339-341.
13. Sparber, W., *Entwicklung und Optimierung von Oberflächen-Textur-Verfahren von einkristallinen Silizium-Solarzellen,* in *Fachbereich Technische Physik.* 2003, Technische Universität Graz: Graz. p. 113.
14. Oh, J., H.-C. Yuan, and H.M. Branz, *An 18.2%-efficient black-silicon solar cell achieved through control of carrier recombination in nanostructures.* NATURE NANOTECHNOLOGY, 2012. **7**.
15. Dingemans, G., et al., *Silicon surface passivation by ultrathin Al_2O_3 films synthesized by thermal and plasma atomic layer deposition.* Physica Status Solidi RRL, 2010. **4**(1-2): p. 10-2.
16. Kern, W., *Handbook of semiconductor wafer cleaning technology.* 1993, Park Ridge, New Jersey: Noyes. 623.
17. A.W.Stephens, A.G.Aberle, and M.A.Green, *Surface recombination velocity measurements at the silicon-silicon dioxide interface by microwave-detected photoconductance decay.* J.Appl.Phys., 1994. **76**(1): p. 363.
18. Glatthaar, M., et al., *Spatially resolved determination of dark saturation current and series resistance of silicon solar cells.* Physica Status Solidi RRL, 2010. **4**(1): p. 13-15.
19. U.Jäger, et al., *Influence of doping profile of highly doped regions for selective emitter solar cells,* in *35th IEEE Photovoltaic Spec. Conf.* 2010: Honolulu. p. 003185 - 003189.